Inorganic Chemistry

including bioinorganic chemistry

August 18, 2014
Volume 53, Number 16
pubs.acs.org/IC

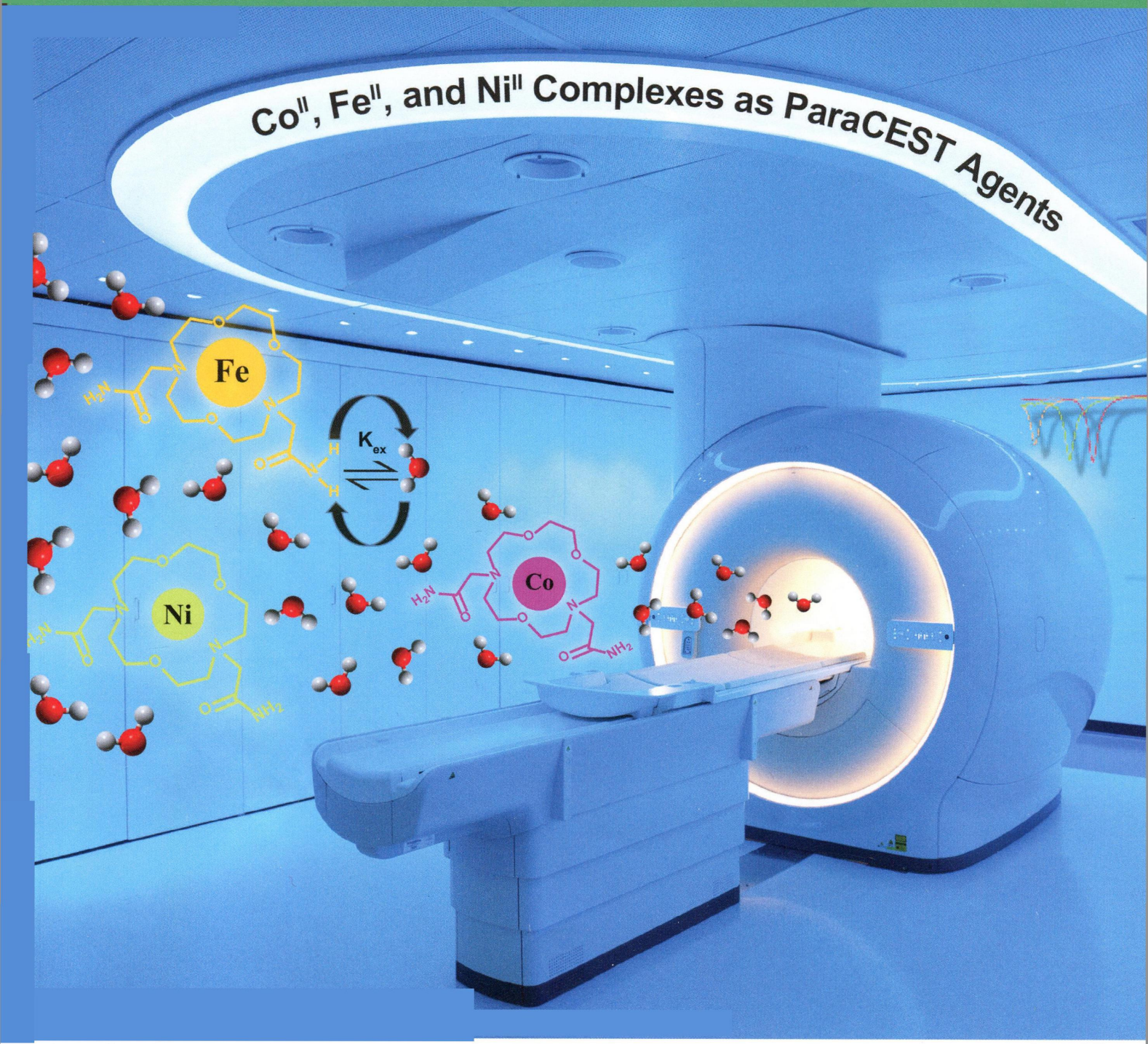

Inorganic Chemistry

AUGUST 18, 2014
VOLUME 53 ISSUE 16

INOCAJ 53(16) 8191–8838 (2014)
ISSN 0020-1669
Registered in the U.S. Patent and Trademark Office

ON THE COVER: Amide-appended macrocyclic complexes of iron(II), cobalt(II), and nickel(II) function as paramagnetic chemical exchange saturation transfer (paraCEST) MRI contrast agents in rabbit serum and in tissue mimics. The reactivity of the three metal ion complexes in serum correlates with the coordination geometry of the complexes. See A. O. Olatunde, J. M. Cox, M. D. Daddario, J. A. Spernyak, J. B. Benedict, and J. R. Morrow, p 8311.

Communications

8197 (S) dx.doi.org/10.1021/ic501444t

$Ca_3Na_4LiBe_4B_{10}O_{24}F$: A New Beryllium Borate with a Unique Beryl Borate $^2_\infty[Be_8B_{16}O_{40}F_2]$ Layer Intrabridged by $[B_{12}O_{24}]$ Groups

Siyang Luo, Wenjiao Yao, Pifu Gong, Jiyong Yao, Zheshuai Lin,* and Chuangtian Chen

A novel beryllium borate, $Ca_3Na_4LiBe_4B_{10}O_{24}F$, has been discovered. It possesses a unique $^2_\infty[Be_8B_{16}O_{40}F_2]$ layer composed of two opposite parallel $[Be_4B_4O_{12}F]_\infty$ layers bridged with $[B_{12}O_{24}]$ polyborates. The linkage of $[B_{12}O_{24}]$ to other structural units is first found in anhydrous borates.

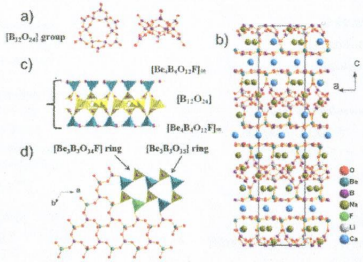

8200 (S) dx.doi.org/10.1021/ic501524a

Single-Molecule Magnetism in a Pentacoordinate Cobalt(II) Complex Supported by an Antenna Ligand

Cyril Rajnák, Ján Titiš, Olaf Fuhr, Mario Ruben, and Roman Boča*

Pentacoordinate complex $[CoL^3Cl_2]$ with a tridentate antenna-like ligand L^3 forms a dimer held by short $\pi-\pi$ stacking with head-to-head contacts at 3.4 Å. The direct-current (dc) magnetic susceptibility and magnetization data confirm weak ferromagnetic interaction and a large-magnetic anisotropy, $D/hc = 150\ cm^{-1}$ and $E/hc = 11.6\ cm^{-1}$. The system shows superparamagnetic behavior at low temperature that depends upon the applied magnetic field. At $B_{dc} = 0.2$ T, a low-frequency peak at the out-of-phase susceptibility is seen ($\nu \sim 0.3$ Hz), whereas the onset of the second peak appears at $\nu > 1500$ Hz, indicating two slow relaxation processes.

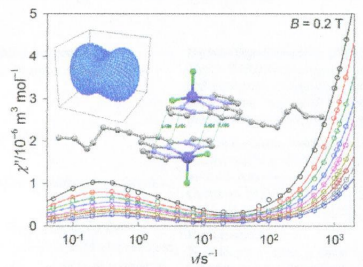

Articles

8203 S dx.doi.org/10.1021/ic500264k

Spin Crossover in Fe(II) and Co(II) Complexes with the Same Click-Derived Tripodal Ligand

David Schweinfurth, Serhiy Demeshko, Stephan Hohloch, Marc Steinmetz, Jan Gerit Brandenburg, Sebastian Dechert, Franc Meyer, Stefan Grimme,* and Biprajit Sarkar*

Weak noncovalent interactions are shown to influence torsion angles at the metal centers which drive spin crossover in Co(II) and Fe(II) complexes with the same click-derived tripodal ligand.

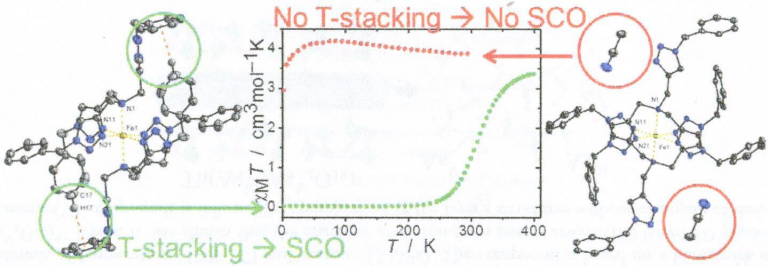

8213 S dx.doi.org/10.1021/ic5002336

New Class of Scorpionate: Tris(tetrazolyl)−Iron Complex and Its Different Coordination Modes for Alkali Metal Ions

Ka Hyun Park, Kang Mun Lee, Min Jeong Go, Sung Ho Choi, Hyoung-Ryun Park, Youngjo Kim,* and Junseong Lee*

A metallascorpionate complex featuring two different binding sites was prepared, and its different coordination modes with alkali metals in solution were studied. A honeycomb-coordinated structure with a one-dimensional infinite metallic array of $-(K-K-Fe-Zn-Fe-K)_n-$ was constructed by assembly of tetrazole and Fe, K, and Zn precursors.

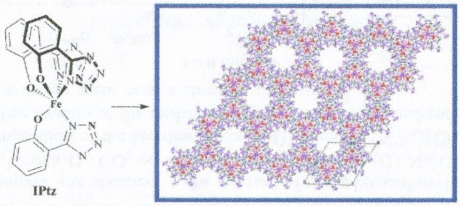

8221 S dx.doi.org/10.1021/ic5002539

Influence of the Electronic Configuration in the Properties of d^6–d^5 Mixed-Valence Complexes

German E. Pieslinger, Bruno M. Aramburu-Trošelj, Alejandro Cadranel, and Luis M. Baraldo*

The cyanide bridged complexes *trans*-$[(T)(bpy)Ru^{II}(\mu\text{-}NC)Ru^{III}L_4(CN)]^{3+}$ (T = 2,2′;6′,2″-terpyridine or tris(1-pyrazolyl)-methane) present contrasting spectroscopies when the pyridine ligand (L) is replaced by 4-methoxypyridine. DFT calculations show that the different spectroscopies arise from the different nature of the acceptor orbital for the IVCT transitions.

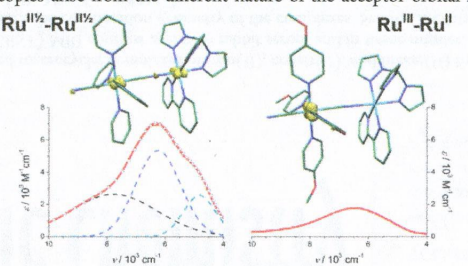

8230 dx.doi.org/10.1021/ic500256a

X-ray Absorption Spectroscopy Systematics at the Tungsten L-Edge

Upul Jayarathne, Perumalreddy Chandrasekaran, Angelique F. Greene, Joel T. Mague, Serena DeBeer, Kyle M. Lancaster, Stephen Sproules,* and James P. Donahue*

A series of six-coordinate tungsten compounds, primarily with phosphine and/or Cl^- ligands and spanning formal oxidation states 0 → +VI, were examined by L-edge X-ray absorption spectroscopy. The estimated branching ratio derived from the L_3- and L_2-edge intensities and the L_1 rising-edge energies correlate with formal oxidation state. The data reported were applied to compounds with ambiguous electronic structure descriptions due to the presence of π-accepting and redox-active ligands.

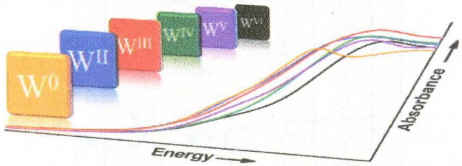

8242 dx.doi.org/10.1021/ic500316w

Cross-dehydrocoupling: A Novel Synthetic Route to P–B–P–B Chains

Souvik Pandey, Peter Lönnecke, and Evamarie Hey-Hawkins*

Transition-metal-catalyzed dehydrocoupling of *tert*-butylferrocenylphosphine–borane [with $[\{Rh(\mu\text{-}Cl)(1,5\text{-}cod)\}_2]$ (cod = cyclooctadiene) as the catalyst] gave the homocoupled product $[Fc(t\text{Bu})(H)P(BH_2)P(Fc)(t\text{Bu})(BH_2X)]$ [Fc = $Fe(C_5H_5)(C_5H_4)$, X = H/Cl], while cross-dehydrocoupling with the tertiary phosphine–boranes $P(t\text{Bu})(n\text{Bu})_2(BH_3)$ and $PPh(n\text{Bu})_2(BH_3)$ using $[Rh(1,5\text{-}cod)_2]OTf$ (OTf = trifluoromethanesulfonate) as the catalyst gave the cross-dehydrocoupled products $[Fc(t\text{Bu})(BH_3)P(BH_2)P(t\text{Bu})(n\text{Bu})_2]$ and $[Fc(t\text{Bu})(BH_3)P(BH_2)PPh(n\text{Bu})_2]$. These compounds seem to be suitable building blocks for the controlled formation of oligomers.

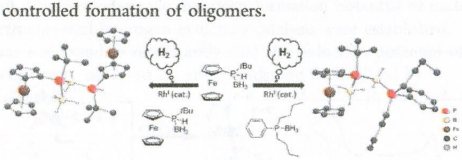

8250 dx.doi.org/10.1021/ic5004269

$Na_{2+x}Ti_6O_{13}$ as Potential Negative Electrode Material for Na-Ion Batteries

Kun Shen and Marnix Wagemaker*

The DFT predicted Na-ion insertion voltage predicts a maximum stoichiometry of $Na_4Ti_6O_{13}$ via a solid solution reaction. Indicated are the crystal structures of the reduced phases at the corresponding Na insertion stages. Yellow spheres represent sodium ion 4i sites, red spheres represent sodium 2d sites, and blue polyhedrons represent the Ti–O octahedra.

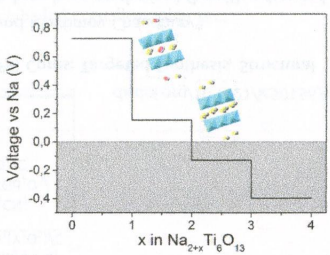

8257 dx.doi.org/10.1021/ic5005177

Relation between the Catalytic Efficiency of the Synthetic Analogues of Catechol Oxidase with Their Electrochemical Property in the Free State and Substrate-Bound State

Prateeti Chakraborty, Jaydeep Adhikary, Bipinbihari Ghosh, Ria Sanyal, Shyamal Kumar Chattopadhyay,* Antonio Bauzá, Antonio Frontera,* Ennio Zangrando,* and Debasis Das*

Experimental investigation followed by theoretical verification establish that rather than the E° values of the original dicopper(II) complexes, the energetics involved in the electrochemical change of the catechol-bound catalysts correlate well with their catalytic efficiency (in terms of k_{cat} values), a new finding in catecholase activity.

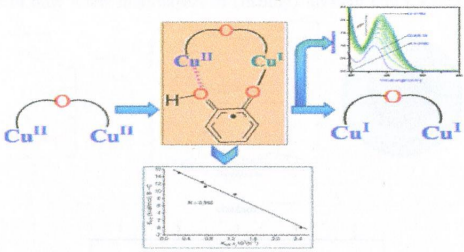

8270 dx.doi.org/10.1021/ic500550y

Polymorph Control of Luminescence Properties in Molecular Crystals of a Platinum and Organoarsenic Complex and Formation of Stable One-Dimensional Nanochannel

Hikaru Unesaki, Takuji Kato, Seiji Watase, Kimihiro Matsukawa, and Kensuke Naka*

The mononuclear diiodoplatinum(II) complex forms three different crystalline polymorphs, which can be either concomitantly or separately obtained on varying the recrystallization conditions. Cubic red crystals (α-phase) and red-orange needles (β-phase) exhibit solid-state red emissions at room temperature. Cubic red crystals of the γ-phase show no solid-state emission at room temperature. In the needlelike crystals of the β-phase, hexagonal arrays of nanoporous channels, 5.0 Å in diameter, formed and encapsulated iodine without distorting the crystal packing.

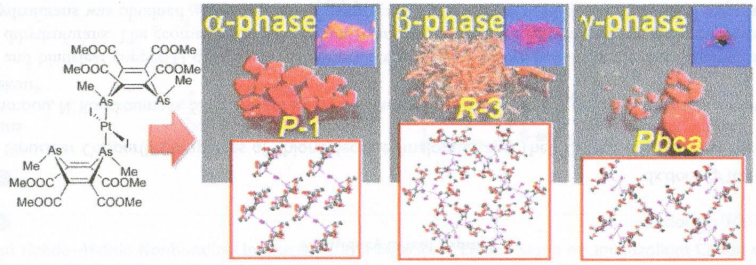

8278 dx.doi.org/10.1021/ic5005769

Coordination Polymer Submicrospheres: Fast Microwave Synthesis and Their Conversion under Different Atmospheres

Shengliang Zhong,* Hongyu Jing, Yuan Li, Shungao Yin, Chenghui Zeng, and Lei Wang*

RE-based coordination polymer (CP) submicrospheres have been prepared via a facile microwave heating method in 5 min. After calcination under different atmospheres and posttreatment, RE_2O_3, REN/RE_2O_3/C, REN/C, $RE_2O_2CN_2$, and carbon submicrospheres can be prepared.

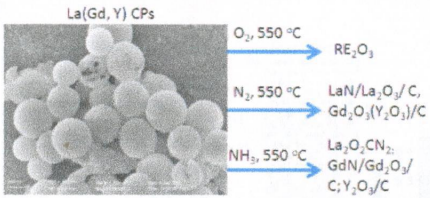

8287 dx.doi.org/10.1021/ic501563r

Heterobimetallic μ-Oxido Complexes Containing Discrete V^V–O–M^{III} (M = Mn, Fe) Cores: Targeted Synthesis, Structural Characterization, and Redox Studies

Kisholoy Bhattacharya, Sk Md Towsif Abtab, Mithun Chandra Majee, Akira Endo, and Muktimoy Chaudhury*

Heterobimetallic compounds (**1**–**7**) containing a $V^V(\mu\text{-O})M^{III}$ (M = Mn, Fe) core have been synthesized through a targeted synthesis route and characterized by X-ray diffraction analysis, electrospray ionization mass spectrometry, and ^{51}V NMR spectroscopy studies. The redox properties of these compounds have been investigated in detail.

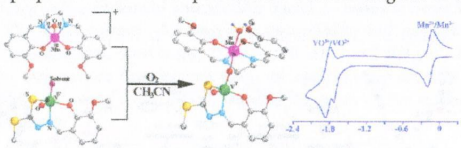

8298 dx.doi.org/10.1021/ic500572p

Influence of the co-Ligand on the Magnetic and Relaxation Properties of Layered Cobalt(II) Thiocyanato Coordination Polymers

Susanne Wöhlert, Zbigniew Tomkowicz, Michał Rams, Stefan G. Ebbinghaus, Lothar Fink, Martin U. Schmidt, and Christian Näther*

In the crystal structure of $[Co(NCS)_2(bpa)]_n$, the cobalt(II) cations are coordinated by four thiocyanato anions and two co-ligands in a distorted octahedral geometry. The cobalt(II) cations are linked into chains by μ-1,3 bridging thiocyanato anions, which are further connected into layers by the 1,2-bis(4-pyridyl)-ethane (bpa) ligand. The compound was magnetically characterized along with the very similar and known compound $[Co(NCS)_2(bpe)]_n$ (bpe = 1,2-bis(4-pyridyl)-ethylene). It was shown that the nature of the co-ligand strongly influenced the static and dynamic magnetic properties.

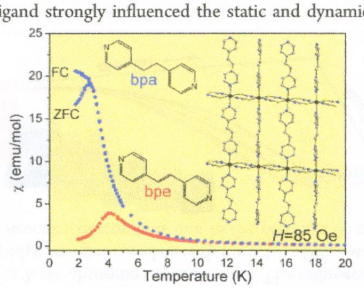

8311 S dx.doi.org/10.1021/ic5006083

Seven-Coordinate Co^{II}, Fe^{II} and Six-Coordinate Ni^{II} Amide-Appended Macrocyclic Complexes as ParaCEST Agents in Biological Media

Abiola O. Olatunde, Jordan M. Cox, Michael D. Daddario, Joseph A. Spernyak, Jason B. Benedict, and Janet R. Morrow*

The crystal structures, solution chemistry, and CEST properties of Fe^{II}, Co^{II}, and Ni^{II} complexes of 7,13-bis(carbamoylmethyl)-1,4,10-trioxa-7,13-diazacyclopentadecane ligand (**L**) in rabbit serum, 4% agarose, egg white, and buffer solutions are compared. The $[Ni(L)]^{2+}$ complex is the most reactive of all the complexes in serum and egg white, corresponding to the misfit of the Ni^{II} ion in the macrocyclic ligand cavity.

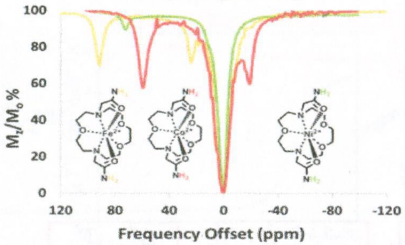

8322 S dx.doi.org/10.1021/ic500727z

Mono- and Binuclear Copper(I) Complexes of Thionucleotide Analogues and Their Catalytic Activity on the Synthesis of Dihydrofurans

D. C. Charalampou, N. Kourkoumelis, S. Karanestora, L. P. Hadjiarapoglou, V. Dokorou, S. Skoulika, A. Owczarzak, M. Kubicki, and S. K. Hadjikakou*

The mono- and binuclear copper(I) complexes of thionucleotide analogues were used to study their catalytic activity on the synthesis of dihydrofurans. The geometry and halogen and ligand types affect the catalytic affinity of the catalysts. The highest yield of dihydrofurans was obtained when the "linear" complexes **1** and **2** were used as the catalysts. Computational studies have shown that the increased chemical stability of **1** and **2** affects their catalytic activity by remaining active over longer periods compared to **3**–**5**.

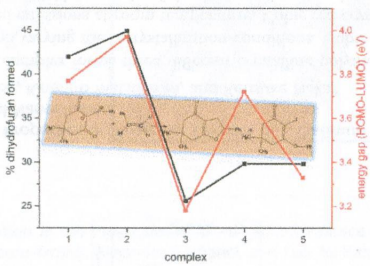

8334 S dx.doi.org/10.1021/ic500743u

A Metathesis Model for the Dehydrogenative Coupling of Amines with Alcohols and Esters into Carboxamides by Milstein's [Ru(PNN)(CO)(H)] Catalysts

Faraj Hasanayn* and Hassan Harb

DFT calculations identify direct outer-sphere pathways that exchange the amide of the octahedral [Ru(PNN)(CO)(H)-(NHMe)] with a hydride from an aldehyde or an alkoxide from an ester. Consideration of these reactions affords a simple metathesis alternative to the generally accepted metal–ligand cooperation mechanism in the dehydrogenative coupling of amines with alcohols and esters into carboxamides using Milstein's catalysts.

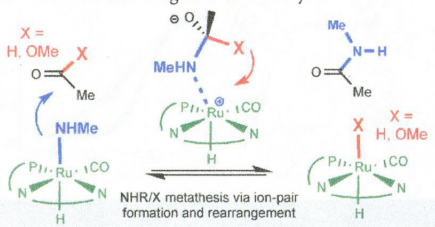

8350 S dx.doi.org/10.1021/ic500770k

Electrochemical Reduction of Brønsted Acids by Glassy Carbon in Acetonitrile—Implications for Electrocatalytic Hydrogen Evolution

Brian D. McCarthy, Daniel J. Martin, Eric S. Rountree, Alexander C. Ullman, and Jillian L. Dempsey*

The electroreduction of 20 acids plus water on glassy carbon was investigated in acetonitrile. With these data and estimates of the thermodynamic hydrogen formation potential of each acid, potential windows for electrochemical hydrogen evolution catalysis were established. The presence of added water was not found to significantly shift the reduction potential of any acid, although current increases were observed for some acids and rationalized by considering conjugate base stabilization.

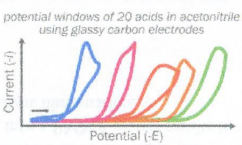

8362 S dx.doi.org/10.1021/ic500773b

$Bi_3Cr_{2.91}O_{11}$: A Ferromagnetic Insulator from Cr^{4+}/Cr^{5+} Mixing

Wei Yi, Yoshitaka Matsushita, Akira Sato, Kosuke Kosuda, Michiko Yoshitake, and Alexei A. Belik*

$Bi_3Cr_{2.91}O_{11}$ belongs to the rare family of ferromagnetic insulators with T_C = 220 K. $Bi_3Cr_{2.91}O_{11}$ was synthesized at high pressure of 6 GPa and high temperature of 1500 K. Its crystal structure and properties were studied using single crystals. $Bi_3Cr_{2.91}O_{11}$ has almost a 1:1 mixture of Cr^{4+} and Cr^{5+} ions distributed in one octahedral crystallographic site.

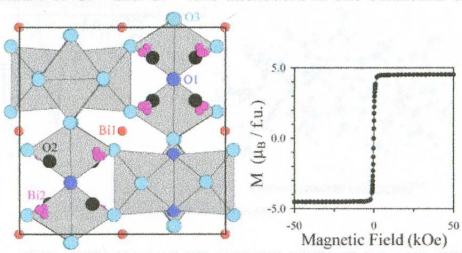

8367 dx.doi.org/10.1021/ic5000183

Site-Selective High-Resolution X-ray Absorption Spectroscopy and High-Resolution X-ray Emission Spectroscopy of Cobalt Nanoparticles

Timna-Josua Kühn,* Josef Hormes, Nina Matoussevitch, Helmut Bönnemann, and Pieter Glatzel

Cobalt nanoparticles (diameter = 6 nm) were characterized by a combination of HRFD-XANES/EXAFS and HR-XES at the cobalt K-edge, using $K\beta_{1,3}$ and $K\beta_{2,5}$ fluorescence. With the help of a numerical procedure and multiple-scattering based simulations, the nanoparticles' core and shell could be described separately. The core was found to have a bulk Co metal-like HCP phase and the shell to be of only a few monolayers of (mainly) divalent CoO, $CoCO_3$, and one further component.

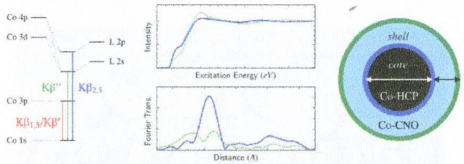

8376 dx.doi.org/10.1021/ic500822w

Cu_3I_7 Trimer and Cu_4I_8 Tetramer Based Cuprous Iodide Polymorphs for Efficient Photocatalysis and Luminescent Sensing: Unveiling Possible Hierarchical Assembly Mechanism

Shi-Li Li and Xian-Ming Zhang*

Two 24-membered-ring-based semiconducting $Cu_{11}I_{17}^{6-}$ open-network polymorphs were generated via solvothermal reactions. In two polymorphs, the basic secondary building units (SBUs) are tetramer Cu_4I_8 and trimeric Cu_3I_7 SBUs that can further fuse into hexameric tertiary building units Cu_6I_{12} and even dodecameric quaternary building units $Cu_{12}I_{22}$. On the basis of these observations, a hierarchical model for forming and assembling copper halide polymorphs has been proposed.

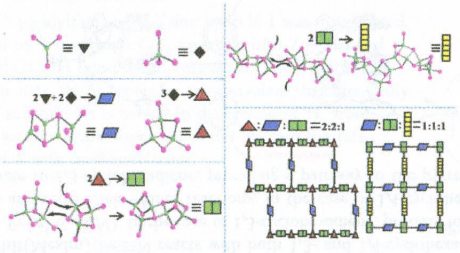

8384 dx.doi.org/10.1021/ic500882z

Anion–π and Halide–Halide Nonbonding Interactions in a New Ionic Liquid Based on Imidazolium Cation with Three-Dimensional Magnetic Ordering in the Solid State

Abel García-Saiz, Imanol de Pedro,* Pedro Migowski, Oriol Vallcorba, Javier Junquera, Jesús Angel Blanco, Oscar Fabelo, Denis Sheptyakov, Joao Carlos Waerenborgh, María Teresa Fernández-Díaz, Jordi Rius, Jairton Dupont, Jesús Antonio Gonzalez, and Jesús Rodríguez Fernández

We present the first magnetic ionic liquid with anion–π interactions, which displays a three-dimensional magnetic ordering below the Néel temperature, T_N = 7.7 K. In this material, called Dimim[$FeBr_4$], an exhaustive and systematic study of the magneto–structural correlations, involving crystal and magnetic structure, physical characterization, and first-principles analysis (DFT simulation), was performed.

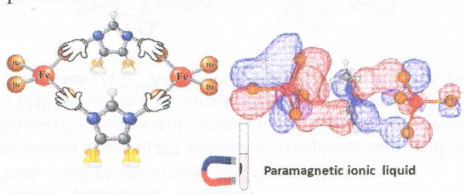

8397 Ⓢ dx.doi.org/10.1021/ic500940a

Platinum Acetate Blue: Synthesis and Characterization

Natalia V. Cherkashina, Dmitry I. Kochubey, Vladislav V. Kanazhevskiy, Vladimir I. Zaikovskii, Vladimir K. Ivanov, Alexander A. Markov, Alla P. Klyagina, Zhanna V. Dobrokhotova, Natalia Yu. Kozitsyna, Igor B. Baranovsky, Olga G. Ellert, Nikolai N. Efimov, Sergei E. Nefedov, Vladimir M. Novotortsev, Michael N. Vargaftik,* and Ilya I. Moiseev

A noncrystalline platinum acetate blue (PAB) of the empirical formula $Pt(OOCMe)_{2.5\pm0.25}$ was proposed as an easily prepared starting material instead of the crystalline platinum(II) acetate. Three new platinum(II) and (III) complexes: $Pt^{II}(dipy)(OOCMe)_2$, $Pt^{III}{}_2(OOCMe)_4(O_3SPhMe)_2$, and $Pt^{II}(\mu\text{-}OOCMe)_4Co^{II}(OH_2)$ were synthesized using PAB as starting material and structurally characterized with X-ray diffraction analysis. The combined EXAFS, SEM, TEM, XRD, DTA-TG, magnetochemical, and DFT−MM+ study revealed the chemical nature of the PAB with the main structural unit $Pt_9(OOCMe)_{23}$.

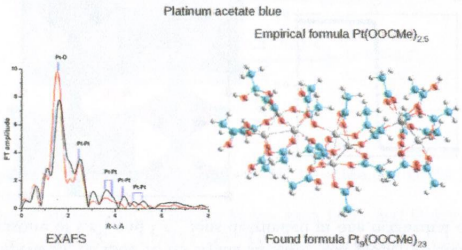

8407 Ⓢ dx.doi.org/10.1021/ic500966z

A Eu^{III} Tetrakis(β-diketonate) Dimeric Complex: Photophysical Properties, Structural Elucidation by Sparkle/AM1 Calculations, and Doping into PMMA Films and Nanowires

Silvanose Biju,* Ricardo O. Freire, Yu Kyung Eom, Rosario Scopelliti, Jean-Claude G. Bünzli,* and Hwan Kyu Kim*

A red-emitting dimeric Eu^{III} podate based on a tetrakis(β-diketonate) ligand emits highly monochromatic red light and features the highest quantum yield reported so far for dinuclear Eu^{III} bis(β-diketonates); doping into a PMMA matrix results in thin films and one-dimensional nanowires, the luminescence of which can be seen under sunlight illumination.

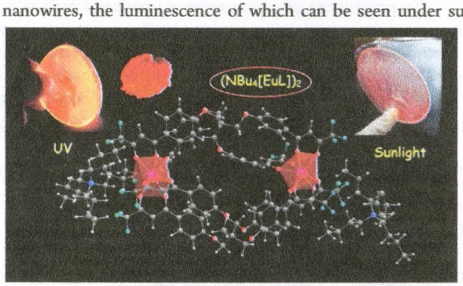

8418 dx.doi.org/10.1021/ic501011p

Uranium(IV) Halide (F^-, Cl^-, Br^-, and I^-) Monoarene Complexes

Dominik P. Halter, Henry S. La Pierre, Frank W. Heinemann, and Karsten Meyer*

The syntheses of four nearly isostructural uranium(IV) monoarene complexes, supported by the arene anchored tris(aryloxide) chelate, $[(^{Ad,Me}ArO)_3mes]^{3-}$, are reported. Oxidation of the uranium(III) precursor $[((^{Ad,Me}ArO)_3mes)U]$, **1**, in the presence of tetrahydrofuran (THF) results in THF coordination and distortion of the equatorial coordination sphere to afford the uranium(IV) η^6-arene complexes, $[((^{Ad,Me}ArO)_3mes)U(X)(THF)]$, **2–X–THF**, (where X = F, Cl, Br, or I) as their THF adducts.

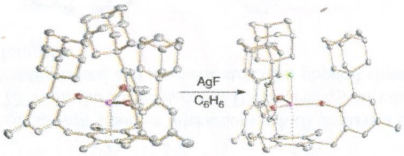

8425 dx.doi.org/10.1021/ic5010006

Reaction of an Iron(IV) Nitrido Complex with Cyclohexadienes: Cycloaddition and Hydrogen-Atom Abstraction

Wei-Tsung Lee, Ruth A. Juarez, Jeremiah J. Scepaniak, Salvador B. Muñoz III, Diane A. Dickie, Haobin Wang,* and Jeremy M. Smith*

The iron(IV) nitrido complex $PhB(MesIm)_3Fe{\equiv}N$ reacts with both 1,3- and 1,4-cyclohexadiene to yield the iron(II) pyrrolide complex, $PhB(MesIm)_3Fe(\eta^5\text{-}C_4H_4N)$. In the case of 1,3-cyclohexadiene, product formation is proposed to occur by sequential [4 + 1] cycloaddition and retro Diels–Alder reactions. In the case of 1,4-cyclohexadiene, initial hydrogen-atom abstraction isomerizes the substrate to 1,3-cyclohexadiene, providing a pathway to the pyrrolide product.

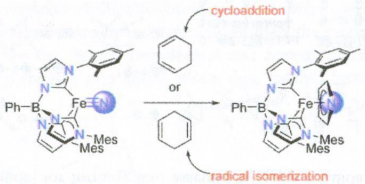

8431 dx.doi.org/10.1021/ic501053v

Manganese-Substituted Rare-Earth Zinc Arsenides $RE_{1-y}Mn_xZn_{2-x}As_2$ (*RE* = Eu–Lu) and $RE_{2-y}Mn_xZn_{4-x}As_4$ (*RE* = La–Nd, Sm, Gd)

Xinsong Lin, Danisa Tabassum, Brent W. Rudyk, and Arthur Mar*

Manganese substitution permits defect $CaAl_2Si_2$-type structures to form for nearly all rare-earth components, with development of partial ordering and superstructures.

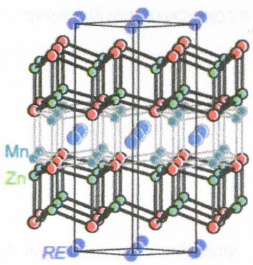

8442 S dx.doi.org/10.1021/ic5010159

Spin Crossover Star-Shaped Metallomesogens of Iron(II)

Maksym Seredyuk,* M. Carmen Muñoz, Vadim Ksenofontov, Philipp Gütlich, Yury Galyametdinov, and Jose A. Real*

Magnetic, calorimetric, Mössbauer, single-crystal and powder X-ray studies of a new series of star-shaped iron(II) spin crossover (SCO) complexes with variable-length alkyl chains are reported. Long chain species display SCO properties and liquid crystal properties.

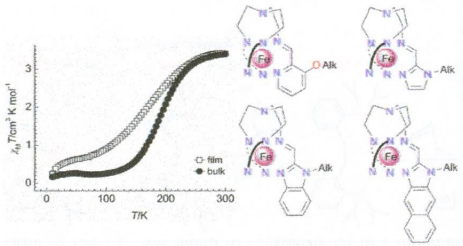

8455 S dx.doi.org/10.1021/ic501034b

Reactivity of Organothorium Complexes with TEMPO

Ryan R. Langeslay, Justin R. Walensky, Joseph W. Ziller, and William J. Evans*

Organothorium alkyl, allyl, hydride, and bromide complexes react with the TEMPO radical to cleanly generate new complexes of TEMPO$^-$ anions in both η^1- and η^2-coordination modes. $(C_5Me_5)^-$ ligands can be removed by TEMPO as shown, and thorium tetrabromide forms a radical adduct of TEMPO.

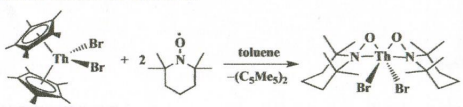

8464 S dx.doi.org/10.1021/ic501036h

On the Possibility of Magneto-Structural Correlations: Detailed Studies of Dinickel Carboxylate Complexes

James P. S. Walsh, Stephen Sproules, Nicholas F. Chilton, Anne-Laure Barra, Grigore A. Timco, David Collison,* Eric J. L. McInnes, and Richard E. P. Winpenny

Magneto-structural correlations obscured by large zero-field splitting effects in a family of nickel dimers were elucidated through an approach that combined high-field high-frequency EPR with magnetic and optical absorption measurements.

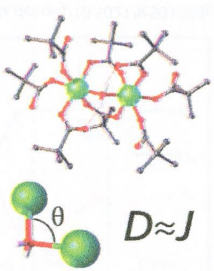

8473 S dx.doi.org/10.1021/ic501029b

High-Pressure and Theoretical Studies Reveal Significant Differences in the Electronic Structure and Bonding of Magnesium, Zinc, and Nickel Ions in Metalloporphyrinoids

Agnieszka Kania, Mariusz Pilch, Dorota Rutkowska-Zbik, Anna Susz, Heriyanto, Grażyna Stochel, and Leszek Fiedor*

Chemical bonding between the central metal ion and porphyrinoids depends on both the electronic configuration of the central ion and the symmetry of electron distribution in the central binding pocket. Theoretical and spectroscopic analysis shows that in most cases it is not a coordinative bond. In all metalloporphyrinoids having no inversion center (C_1, C_2 and C_{2v} symmetry), the central Mg^{2+}, Zn^{2+}, and Ni^{2+} ions are bound via ionic, coordinative, and covalently coordinative bonds, respectively.

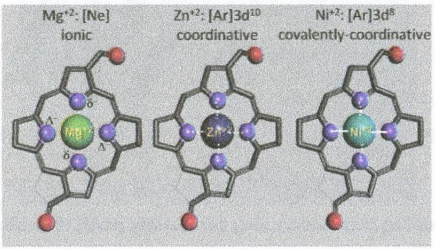

8485 S dx.doi.org/10.1021/ic501058j

Generation of Dihydrogen Molecule and Hydrosilylation of Carbon Dioxide Catalyzed by Zinc Hydride Complex: Theoretical Understanding and Prediction

Milind Madhusudan Deshmukh* and Shigeyoshi Sakaki*

Multifunctional catalysis of [tris(2-pyridylthio)methyl]zinc hydride **1** was investigated. Hydrosilylation of CO_2 catalyzed by **1** occurs via CO_2 insertion into Zn−H bond followed by metathesis of Zn−η^1-OCOH bond with hydrosilane. The metathesis is rate-determining. In the transition state, the Si center has a hypervalent structure. Only hydrosilane with electronegative substituents is useful. In generation of H_2 from methanol/water catalyzed by **1**, various hydrosilanes are useful because the rate-determining step is metathesis of **1** with methanol/water.

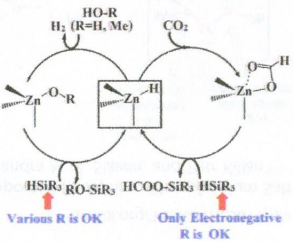

8494 S dx.doi.org/10.1021/ic501060w

Thermodynamics of the Cu^{II} μ-Thiolate and Cu^{I} Disulfide Equilibrium: A Combined Experimental and Theoretical Study

Erica C.M. Ording-Wenker, Martijn van der Plas, Maxime A. Siegler, Sylvestre Bonnet, F. Matthias Bickelhaupt, Célia Fonseca Guerra,* and Elisabeth Bouwman*

The redox equilibrium between dinuclear Cu^{II} μ-thiolate and Cu^{I} disulfide structures has been studied. It was found that the equilibrium between the two species can depend on both solvent and temperature, and that the μ-thiolate complex forms under kinetic control, whereas the disulfide complex is the most stable species. The energies of the μ-thiolate and disulfide complexes for two series of related ligands have been calculated with DFT; the results rationalize the experimentally observed structures.

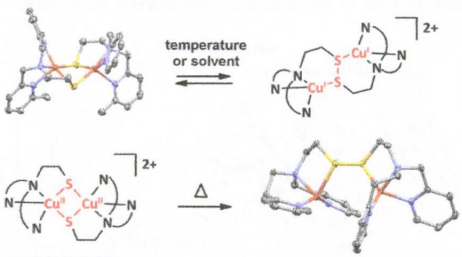

8505 S dx.doi.org/10.1021/ic501080c

Multicopper Models for the Laccase Active Site: Effect of Nuclearity on Electrocatalytic Oxygen Reduction

Edmund C. M. Tse, David Schilter, Danielle L. Gray, Thomas B. Rauchfuss, and Andrew A. Gewirth*

Enzymes containing multiple copper ions catalyze the four-electron reduction of dioxygen to water very efficiently. To mimic the catalytic performance of the enzymes, we connected two copper-bearing 2,2′-dipicolylamine units together with an alkyl linker, and installed a third metal-binding pocket in the ligand framework.

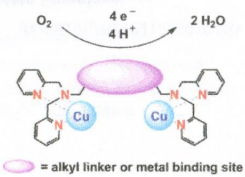

8517 S dx.doi.org/10.1021/ic5010566

Flexible Coordination of Diphosphine Ligands Leading to cis and trans Pd(0), Pd(II), and Rh(I) Complexes

Cezar C. Comanescu and Vlad M. Iluc*

A series of diphosphine ligands was investigated to determine the preference for cis/trans coordination. Increasing the length of the bridging alkyl backbone from one to two carbons changes the geometry of the resulting palladium(II) complexes, with L^1 coordinating cis, while L^2 coordinates in a trans fashion. Coordination to Pd(0) leads to complexes in which both ligands accommodate a P–M–P angle close to 120°. L^2 was found to coordinate cis in a rhodium(I) complex.

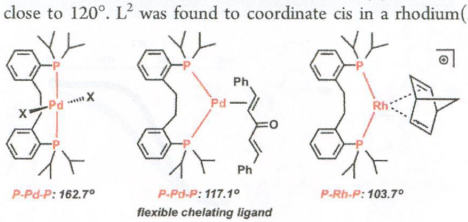

8529 dx.doi.org/10.1021/ic5011133

Surfactant Media To Grow New Crystalline Cobalt 1,3,5-Benzenetricarboxylate Metal–Organic Frameworks

Hai-Sheng Lu, Linlu Bai, Wei-Wei Xiong, Peizhou Li, Junfeng Ding, Guodong Zhang, Tom Wu, Yanli Zhao, Jong-Min Lee, Yanhui Yang,* Baoyou Geng,* and Qichun Zhang*

Three new Co-MOFs (**NTU-Z30**, **NTU-Z31**, and **NTU-Z32**) were synthesized under surfactant media. The topology studies indicate that **NTU-Z30** and **NTU-Z32** possess two new topologies, 3,3,6,7-c net and 2,8-c net, respectively, while **NTU-Z31** has a known topology **rtl** type (3,6-c net). The magnetic analyses show that all three materials have weak antiferromagnetic behavior. Furthermore, **NTU-Z30** has been selected as the heterogeneous catalyst for the aerobic epoxidation of alkene, and our results show that this material exhibits excellent catalytic activity as well as good stability.

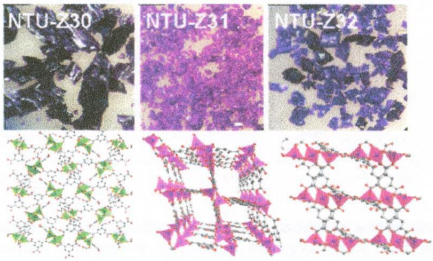

8538 dx.doi.org/10.1021/ic501142v

Synthetic and Structural Study of the Coordination Chemistry of a *peri*-Backbone-Supported Phosphino-Phosphonium Salt

Matthew J. Ray, Michael Bühl, Laurence J. Taylor, Kasun S. Athukorala Arachchige, Alexandra M. Z. Slawin, and Petr Kilian*

Acenaphthene *peri*-backbone-supported phosphino-phosphonium chloride shows three distinct modes of reactivity in reactions with metal fragments, including η^1 coordination, chloride transfer to phosphenium, and reduction of phosphenium to a phosphido group.

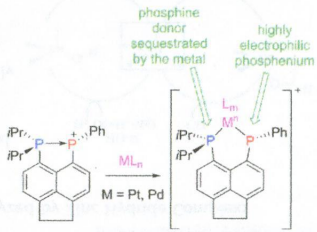

8548 dx.doi.org/10.1021/ic501128n

Synthesis of PbS/PbI_2 Nanocomposites in Mixed Solvent and Their Composition-Dependent Electrogenerated Chemiluminescence Performance

Suli Liu, Long Zhang, Yanrong Li, Min Han, Zhihui Dai,* and Jianchun Bao*

PbS/PbI_2 nanocomposites were prepared by choosing $K[PbI_3]$ as both a lead salt and an iodide precursor and acetone/water as a reaction medium, which exhibited good and composition-dependent electrogenerated chemiluminescence performance.

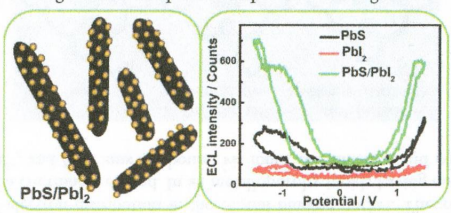

8555 S dx.doi.org/10.1021/ic501163x

Dimensional and Coordination Number Reductions in a Large Family of Lanthanide Tellurite Sulfates
Jian Lin, Kariem Diefenbach, Naoki Kikugawa, Ryan E. Baumbach, and Thomas E. Albrecht-Schmitt*

A large family of 22 lanthanide tellurite sulfates with five different topologies has been prepared. Their structures have been elucidated, and magneto-structural correlations and luminscent properties have been developed.

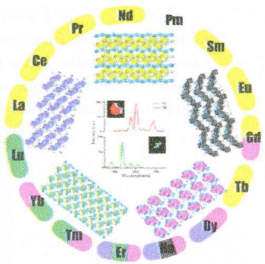

8565 S dx.doi.org/10.1021/ic501146r

Bioinspired Magneto-optical Bacteria
Fernando Carmona, Miguel Martín, Natividad Gálvez, and Jose M. Dominguez-Vera*

Living magneto-optical bacteria have been produced for the first time by incorporating iron oxide and gold nanoparticles onto probiotic (and healthy) bacteria.

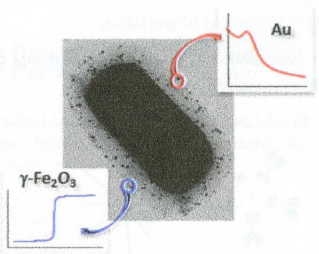

8570 S dx.doi.org/10.1021/ic5011506

Microwave-Assisted Solvothermal Synthesis of Spinel AV_2O_4 (M = Mg, Mn, Fe, and Co)
Arturo Gutierrez and Arumugam Manthiram*

A qualitative energy diagram showing the shifting of energy levels on bringing together the ions to form a crystalline solid. Lower-valent spinel AV_2O_4 containing A^{2+} and V^{3+} ions can be synthesized in tetraethylene-glycol (TEG) medium as the energy of the cations in solution is lower than the HOMO of TEG. The samples were synthesized in 30 min at 300 °C.

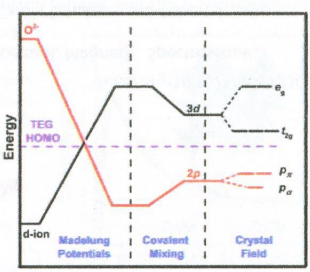

8577 dx.doi.org/10.1021/ic501168a

Magnetic Resonance Properties of Actinyl Carbonate Complexes and Plutonyl(VI)-tris-nitrate

Frédéric Gendron, Ben Pritchard, Hélène Bolvin, and Jochen Autschbach*

The electronic structures and magnetic properties of actinyl ions AnO_2^{n+} (An = U, Np, and Pu), equatorially coordinated tris-carbonate complexes thereof, and plutonyl-tris-nitrate are investigated theoretically. The results are rationalized with the help of crystal-field models extracted from the ab initio calculations, and by generating natural orbital and natural spin orbitals contributing to the magnetic properties and the unpaired spin distributions.

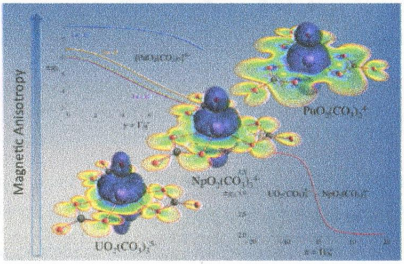

8593 dx.doi.org/10.1021/ic501178f

4,4′,5,5′-Tetracarboxy-2,2′-bipyridine Ru(II) Sensitizers for Dye-Sensitized Solar Cells

Chun-Cheng Chou, Fa-Chun Hu, Kuan-Lin Wu, Tainan Duan, Yun Chi,* Shih-Hung Liu, Gene-Hsiang Lee, and Pi-Tai Chou*

Ru(II) sensitizers bearing the 4,4′,5,5′-tetracarboxy-2,2′-bipyridine anchor were prepared, showing inferior efficiency versus their 4,4′-dicarboxy counterparts possibly due to the enhanced deprotonation and the perpendicularly oriented central carboxyl groups.

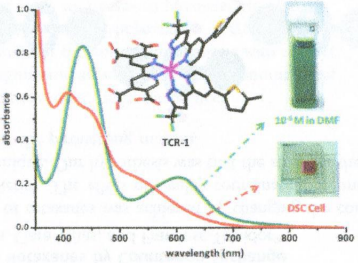

8600 dx.doi.org/10.1021/ic501210t

Electrochemistry and Catalytic Properties for Dioxygen Reduction Using Ferrocene-Substituted Cobalt Porphyrins

Bin Sun, Zhongping Ou,* Deying Meng, Yuanyuan Fang, Yang Song, Weihua Zhu, Pavlo V. Solntsev, Victor N. Nemykin,* and Karl M. Kadish*

Four *meso*-substituted cobalt porphyrins containing zero, one, three, and four ferrocenyl groups were synthesized and examined as to their electrochemical properties in *N*,*N*′-dimethylformamide or 1.0 M $HClO_4$. Each porphyrin was also examined as to its ability to catalytically reduce dioxygen when adsorbed on the surface of a graphite electrode. The effect of the ferrocenyl groups on the redox potentials and dioxygen reduction products are discussed.

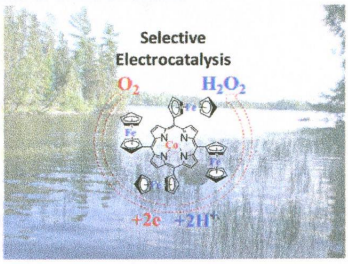

8610 S dx.doi.org/10.1021/ic501224q

Exploring the Coordination Chemistry of 3,3′-Di(picolinamoyl)-2,2′-bipyridine: One Ligand, Multiple Nuclearities

Nicholas J. Hurley, John J. Hayward, Jeremy M. Rawson, Mark Murrie, and Melanie Pilkington*

The coordination chemistry of a polydentate, 3,3′-disubstituted bipyridine ligand is discussed, revealing its propensity to form a range of multinuclear complexes that include trimeric and tetrameric cluster topologies, as well as a 1-D chain with varying coordination isomerism.

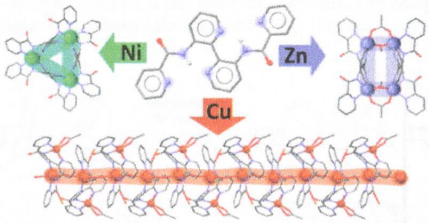

8624 S dx.doi.org/10.1021/ic501236j

Thiocyanate Complexes of Uranium in Multiple Oxidation States: A Combined Structural, Magnetic, Spectroscopic, Spectroelectrochemical, and Theoretical Study

Emtithal Hashem, James A. Platts, František Hartl, Giulia Lorusso, Marco Evangelisti, Carola Schulzke, and Robert J. Baker*

Uranium thiocyanate complexes in different oxidation states have been studied by SQUID magnetometry, photoluminescence spectroscopy, and spectroelectrochemistry. The magnetic properties of $[U(NCS)_8]^{4-}$ have been studied with respect to the geometry around the uranium ion. The thiocyanate ligands in this complex have been found to undergo unusual anodic reactivity.

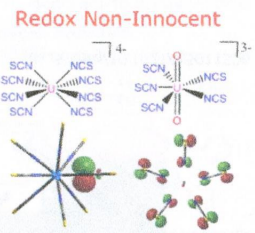

8638 S dx.doi.org/10.1021/ic501238u

A Bifunctional Cr/Yb/Tm:$Ca_3Ga_2Ge_3O_{12}$ Phosphor with Near-Infrared Long-Lasting Phosphorescence and Upconversion Luminescence

Daqin Chen,* Yan Chen, Hongwei Lu, and Zhenguo Ji

$Cr^{3+}/Yb^{3+}/Tm^{3+}$ triply doped $Ca_3Ga_2Ge_3O_{12}$ is demonstrated to be a novel bifunctional near-infrared long-lasting phosphorescence and upconversion luminescence material. Impressively, the addition of lanthanide ions into $Cr:Ca_3Ga_2Ge_3O_{12}$ can greatly increase the Cr^{3+} afterglow time due to the formation of extra deeper traps.

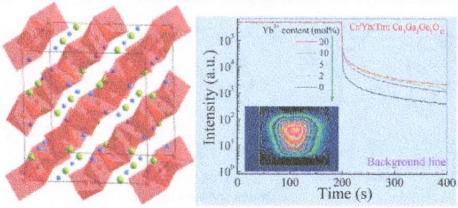

8646 dx.doi.org/10.1021/ic5012346

Solid-State NMR and Raman Spectroscopy To Address the Local Structure of Defects and the Tricky Issue of the Cu/Zn Disorder in Cu-Poor, Zn-Rich CZTS Materials

Michaël Paris,* Léo Choubrac, Alain Lafond, Catherine Guillot-Deudon, and Stéphane Jobic

Cu-poor, Zn-rich CZTS powdered samples are characterized using solid-state NMR and Raman spectroscopy. We focus our attention on the structures of $[V_{Cu} + Zn_{Cu}]$ and $[2Zn_{Cu} + Zn_{Sn}]$ defect complexes and their impact on the long-range Cu/Zn disorder.

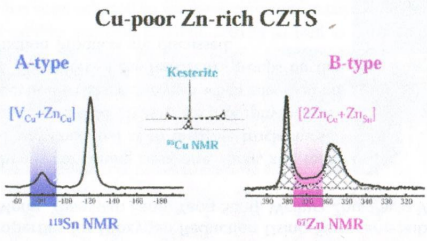

8654 dx.doi.org/10.1021/ic501246e

Controlling the Pirouetting Motion in Rotaxanes by Counterion Exchange

Pau Farràs,* Eduardo C. Escudero-Adán, Clara Viñas, and Francesc Teixidor*

Fine tuning of the pirouetting motion of rotaxanes was achieved by changing the counterion of protonated benzylic amide macrocycle-containing fumaramide moieties. The effect of weakly coordinating anions such as metallacarboranes was investigated using the EXSY NMR technique. Our hypothesis was that the stronger the ion pair the lower the rate of rotation, as the anion would act as an anchor for the pirouetting motion.

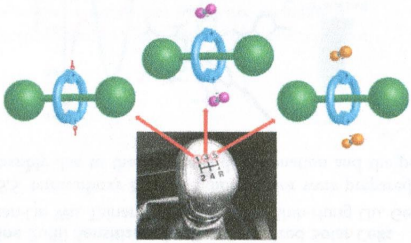

8662 dx.doi.org/10.1021/ic501265k

Application of the Donor–Acceptor Concept to Intercept Low Oxidation State Group 14 Element Hydrides using a Wittig Reagent as a Lewis Base

Anindya K. Swarnakar, Sean M. McDonald, Kelsey C. Deutsch, Paul Choi, Michael J. Ferguson, Robert McDonald, and Eric Rivard*

We report the use of a readily available Wittig reagent $Ph_3P{=}CMe_2$ as a donor to stabilize low coordinate Group 14 element dihydrides.

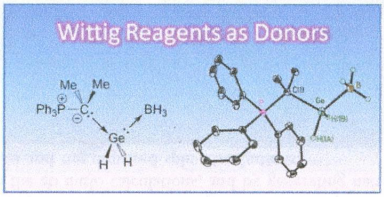

8672 S dx.doi.org/10.1021/ic501286m

Heteroleptic Cyclometalated Iridium(III) Complexes Supported by Triarylborylpicolinate Ligand: Ratiometric Turn-On Phosphorescence Response upon Fluoride Binding

Sanjeev Sharma, Hyungjun Kim, Young Hoon Lee, Taewon Kim, Yoon Sup Lee, and Min Hyung Lee*

Heteroleptic $(C^N)_2Ir(Bpic)$ complexes supported by N^O chelating triarylborylpicolinate (Bpic) ancillary ligand were synthesized and characterized. Fluoride binding to the B atom of the Bpic ligand led to a novel ratiometric turn-on phosphorescence response. Switching of the weakly emissive $^3ML'CT/^3LL'CT$ state to the highly emissive ^3MLCT state centered on the $(C^N)_2Ir$ moiety is suggested to be responsible for the observed turn-on phosphorescence response.

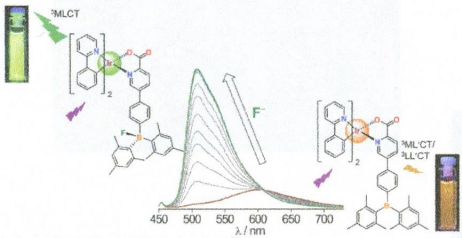

8681 S dx.doi.org/10.1021/ic501293z

Radical or Not Radical: Compared Structures of Metal (M = Ni, Au) Bis-Dithiolene Complexes with a Thiazole Backbone

Agathe Filatre-Furcate, Nathalie Bellec, Olivier Jeannin, Pascale Auban-Senzier, Marc Fourmigué, Antoine Vacher, and Dominique Lorcy*

Comparison of the structure of the neutral, diamagnetic $[Ni(Et\text{-}thiazdt)_2]^0$ with its radical and neutral gold analogue, $[Au(Et\text{-}thiazdt)_2]^\bullet$ demonstrates the role of overlap interactions in the radical gold complex. Despite its closed-shell character, the neutral nickel complex $[Ni(Et\text{-}thiazdt)_2]^0$ exhibits a high room-temperature conductivity $\sigma_{RT} \approx 0.014$ S cm^{-1}.

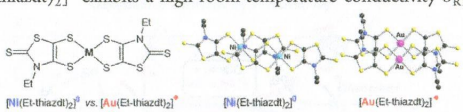

8691 S dx.doi.org/10.1021/ic501308q

Synthesis, Structure, and Properties of the Electron-Poor II–V Semiconductor ZnAs

Andreas Fischer, Daniel Eklöf, Daryn E. Benson, Yang Wu, Ernst-Wilhelm Scheidt, Wolfgang Scherer, and Ulrich Häussermann*

ZnAs can be prepared by high-pressure techniques and is isostructural to thermoelectric ZnSb. Both compounds display a similarly low lattice thermal conductivity above 150 K, which is explained by an accumulation of weakly dispersed optic modes at low energies. Their occurrence is inherent to the electron-poor bonding properties common for both ZnSb and ZnAs.

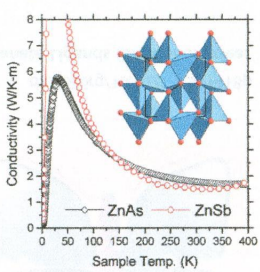

8700 S dx.doi.org/10.1021/ic501334p

Open-Shell Character and Second Hyperpolarizabilities of One-Dimensional Chromium(II) Chains: Size Dependence and Bond-Length Alternation Effect

Hitoshi Fukui, Shota Takamuku, Taishi Yamada, Kotaro Fukuda, Taku Takebayashi, Yasuteru Shigeta, Ryohei Kishi, Benoît Champagne, and Masayoshi Nakano*

Using the spin-unrestricted density functional theory method, we have investigated the longitudinal third-order nonlinear optical properties (the second hyperpolarizabilities γ) of open-shell singlet one-dimensional Cr^{II}_{2n} chains (n = 1–4). The systems display bell-shaped behaviors of γ as a function of the metal–metal bond length, where the γ values attain maxima (dominated by $\gamma(d\sigma)$) for intermediate $d\sigma$ open-shell character. The maximum γ value also exhibits remarkable enhancement as a function of chain length.

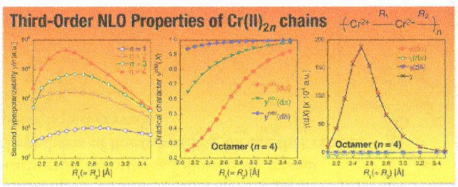

8708 S dx.doi.org/10.1021/ic501336x

$[(C_2H_5)_4N][U_2O_4(HCOO)_5]$, an Ammonium Uranyl Formate Framework Showing Para- to Ferro-Electric Transition: Synthesis, Structures, and Properties

Qianqian Zhu, Ran Shang, Sa Chen, Chunli Liu,* Zheming Wang,* and Song Gao*

An ammonium uranyl formate framework of $[(C_2H_5)_4N][U_2O_4(HCOO)_5]$ possesses a layered structure of anionic wavy sheets and intercalated $(C_2H_5)_4N^+$ cations. Structural "freezing" on cooling leads to a para- to ferro-electric phase transition at ~200 K, with an estimated spontaneous polarization of 0.86 μC cm^{-2} resulting from the concerted and net shifts of the ammonium cations with respect to the anionic sheet, accompanied by significant, anisotropic dielectric anomalies of significant thermal hysteresis and an enhancement in luminescence.

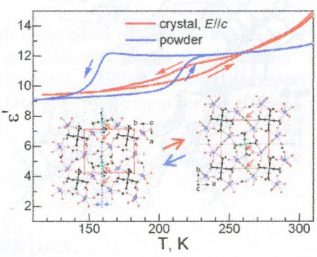

8717 S dx.doi.org/10.1021/ic501324r

^{17}O NMR Study of Diamagnetic and Paramagnetic Lanthanide(III)–DOTA Complexes in Aqueous Solution

Luca Fusaro* and Michel Luhmer

$[Ln\text{-}DOTA]^-$ complexes (Ln ≠ Pm^{3+}, Gd^{3+}) were studied in aqueous solution by ^{17}O NMR. The signals of both the nonchelating (O_1) and chelating (O_2) oxygen atoms could be detected, and the Fermi contact and pseudocontact contributions to the observed lanthanide-induced shifts could be extracted. The results of the study suggest that ^{17}O NMR should prove to be useful for the study of highly paramagnetic Gd(III) complexes of nonlabile ligands.

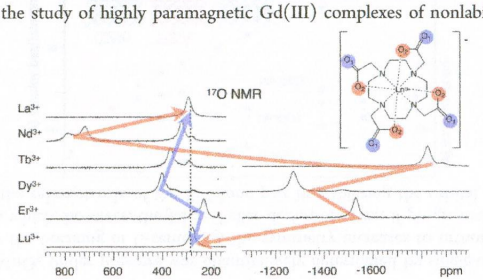

8723 S dx.doi.org/10.1021/ic501353g

Field-Induced Ferromagnetism and Multiferroic Behavior in End-on Pseudohalide-Bridged Dinuclear Copper(II) Complexes with Tridentate Schiff Base Blocking Ligands

Subrata Jana, Bikash Kumar Shaw, Prasanta Bhowmik, Klaus Harms, Michael G. B. Drew, Shouvik Chattopadhyay,* and Shyamal Kumar Saha*

Field-induced long-range ferromagnetic ordering is observed due to $\pi\cdots\pi$ stacking interactions, while compounds having hydrogen-bonding interactions give ferroelectric response, and the coupling between two show unique multiferroic behavior.

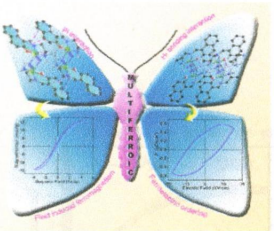

8735 S dx.doi.org/10.1021/ic501418p

Conversion of a Monodentate Amidinate−Germylene Ligand into Chelating Imine−Germanate Ligands (on Mononuclear Manganese Complexes)

Javier A. Cabeza,* Pablo García-Álvarez,* Enrique Pérez-Carreño, and Diego Polo

Manganese complexes containing three-electron-donor imine−germanate ligands have been prepared from a manganese precursor containing a terminal two-electron-donor amidinate−germylene ligand.

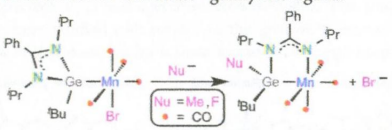

8742 S dx.doi.org/10.1021/ic5013928

Controlling Spin Transition in One-Dimensional Coordination Polymers through Polymorphism

Fernando Novio, Javier Campo, and Daniel Ruiz-Molina*

The influence of polymorphism on spin transition coordination polymers is used to tune the critical interconversion transition temperatures by establishing novel methodologies for the morphology-selective fabrication of coordination polymer microcrystals with reproducible crystalline phases and properties.

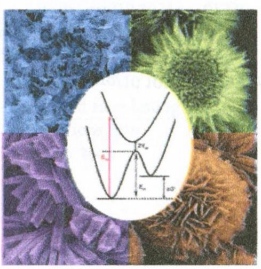

8749 (S) dx.doi.org/10.1021/ic5013878

Structural Evolution under Pressure of $BiMnO_3$

Gianluca Calestani,* Fabio Orlandi, Francesco Mezzadri, Lara Righi, Marco Merlini, and Edmondo Gilioli

The structural evolution of $BiMnO_3$ under pressure was quantitatively determined by single-crystal synchrotron X-ray diffraction up to 36 GPa. After the breaking of C-centering, the symmetry increases to orthorhombic involving a *Pnma* structure similar to $LaMnO_3$ in which, however, the Jahn–Teller distortion, even if progressively reduced, persists up to the highest pressure, pointing out the relevant role of the Bi^{3+} lone pair in stabilizing the orbital order.

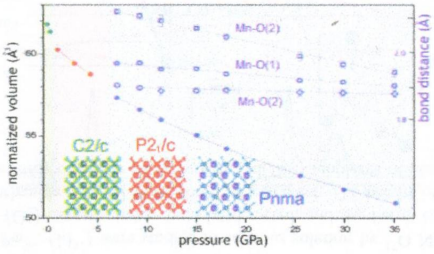

8755 (S) dx.doi.org/10.1021/ic501437g

Hydrogen-Bonding Interactions in a Single-Component Molecular Conductor: a Hydroxyethyl-Substituted Radical Gold Dithiolene Complex

Yann Le Gal, Thierry Roisnel, Pascale Auban-Senzier, Thierry Guizouarn, and Dominique Lorcy*

Gold dithiolene complexes $[Au(EtOH\text{-}thiazdt)_2]^{1-,0}$ bearing two hydroxy groups have been synthesized. Single-crystal X-ray diffraction studies highlight involvement of the hydroxy groups in intermolecular O–H···S hydrogen-bonding interactions. The neutral radical complex $[Au(EtOH\text{-}thiazdt)_2]^{\bullet}$ exhibits a semiconducting behavior under ambient pressure with an activation energy of 0.14 eV. Comparison with the prototypical $[Au(Et\text{-}thiazdt)_2]^{\bullet}$ shows that the hydroxyethyl substituent affects only weakly the overlap interactions, complemented here by added O–H···S hydrogen-bonding interactions.

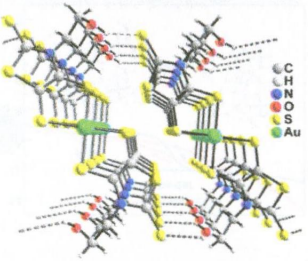

8762 dx.doi.org/10.1021/ic5014494

Practical Synthesis of 1,12-Difunctionalized *o*-Carborane for the Investigation of Polar Liquid Crystals

Aleksandra Jankowiak and Piotr Kaszyński*

Iodination of two 1-substituted *o*-carborane derivatives followed by isomer separation resulted in the practical synthesis of linear building blocks that enable the preparation of new types of polar liquid crystals.

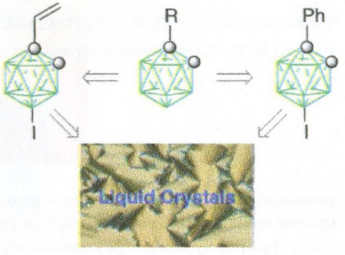

8770 S dx.doi.org/10.1021/ic501458q

Photophysical Responses in Pt_2Pb Clusters Driven by Solvent Interactions and Structural Changes in the Pb^{II} Environment

Jesús R. Berenguer, Elena Lalinde,* Antonio Martín, M. Teresa Moreno,* Santiago Ruiz, Sergio Sánchez, and Hamid R. Shahsavari

The clusters $[\{Pt(C_6F_5)(C^N)\}_2Pb(SpyR\text{-}5)_2]$ exhibit different multistimulus-responsive luminescence and color switches, related to the versatility of the coordination of the Pb^{II} center, modified by $\pi\cdots\pi$ stacking interactions.

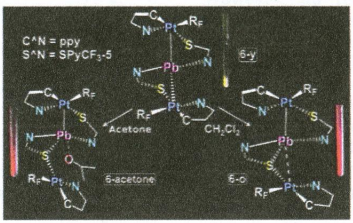

8786 S dx.doi.org/10.1021/ic501461n

Geometric Control of Nuclearity in Copper(I)/Dioxygen Chemistry

Tsukasa Abe, Yuma Morimoto, Tetsuro Tano, Kaoru Mieda, Hideki Sugimoto, Nobutaka Fujieda, Takashi Ogura, and Shinobu Itoh*

Geometric control of nuclearity in copper(I)/dioxygen chemistry has been achieved for the first time by using simple N_3-tridentate ligands bearing a rigid cyclic diamine framework, 1,5-diazacyclooctane (**L8**, eight-membered ring) and 1,4-diazacycloheptane (**L7**, seven-membered ring), with a 2-(2-pyridyl)ethyl side arm, affording completely different dioxygen adducts, a mononuclear copper(II) superoxide complex **S** and a dinuclear copper(III) bis(μ-oxido) complex **O**, respectively. Geometric effects of the supporting ligands are evaluated based on the structural and electrochemical analyses of the copper complexes supported by the related tridentate ligands.

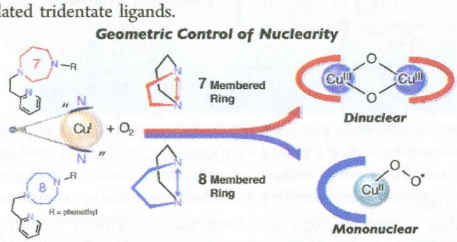

8795 S dx.doi.org/10.1021/ic5014768

Sterically Encumbered Tin and Phosphorus *peri*-Substituted Acenaphthenes

Brian A. Chalmers, Kasun S. Athukorala Arachchige, Joanna K. D. Prentis, Fergus R. Knight, Petr Kilian,* Alexandra M. Z. Slawin, and J. Derek Woollins*

The relationship between attraction and repulsion occurring within sub-van der Waals distances in a number of sterically encumbered *peri*-substituted systems has been investigated. Strained bis(stannanes) [Acenap$(SnR_3)_2$] incorporating bulky tin moieties in the proximal positions have been prepared and their molecular structures compared with those of bis(phosphines) [Acenap$(PR_2)(P^iPr_2)$] and their respective sterically hindered bis(sulfide) derivatives. Metal complexes [{Acenap(PPh_2)-(P^iPr_2)}{$PtCl_2$}] and [{Acenap$(PPh_2)(P^iPr_2)$}{$Mo(CO)_4$}] with typical square planar and octahedral geometries have also been prepared.

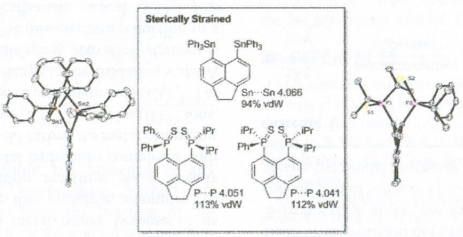

8809 dx.doi.org/10.1021/ic501510u

Platinum Uptake and Ba_2CePtO_6 Formation During in Situ $BaCe_{1-x}M_xO_{3-\delta}$ (M = La, In) Formation

Joey A. Lussier, Shahid P. Shafi, Ronald L. Donaberger, and Mario Bieringer*

We report the formation, structures, temperature-dependent phase transitions, and high-temperature reactivity of the potential proton and oxide ion conductors $BaCe_{1-x}M_xO_3$ (M^{3+} = In^{3+}, La^{3+}). The present in situ diffraction studies show oxidative platinum uptake at temperatures as low as 950 °C into $BaCeO_3$, forming the cubic Ba_2CePtO_6 double perovskite. We report the reaction pathway for the oxidative formation of Ba_2CePtO_6 and the subsequent liberation of platinum for the barium cerate system.

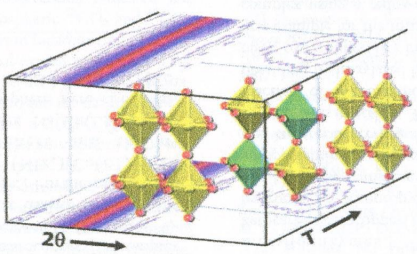

8816 S dx.doi.org/10.1021/ic501548m

$Pb_4V_6O_{16}(SeO_3)_3(H_2O)$, $Pb_2VO_2(SeO_3)_2Cl$, and $PbVO_2(SeO_3)F$: New Lead(II)–Vanadium(V) Mixed-Metal Selenites Featuring Novel Anionic Skeletons

Xue-Li Cao, Fang Kong, Chun-Li Hu, Xiang Xu, and Jiang-Gao Mao*

The combinations of a d^0-V^{5+} cation with the lone-pair-containing cations (Se^{4+} and Pb^{2+}) in the presence of halide anions (Cl^- or F^-) resulted in three new lead(II)–vanadium(V) selenite halides. Their structures feature a 1D $[V_6O_{16}(SeO_3)_3]^{8-}$ branched chain, a 1D $[VO_2(SeO_3)_2]^{3-}$ chain, or a dinuclear $[V_2O_4(SeO_3)_2F_2]^{4-}$ cluster. The polar $Pb_4V_6O_{16}(SeO_3)_3(H_2O)$ displays a weak SHG response of about 0.2 × KDP (KH_2PO_4).

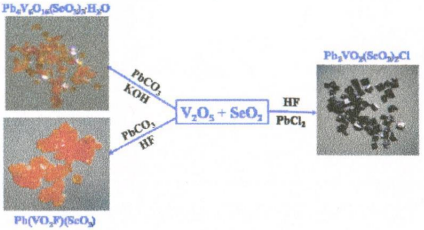

8825 S dx.doi.org/10.1021/ic5017214

Donor–Acceptor Ligand-to-Ligand Charge-Transfer Coordination Complexes of Nickel(II)

Wesley W. Kramer, Lindsay A. Cameron, Ryan A. Zarkesh, Joseph W. Ziller, and Alan F. Heyduk*

A family of charge-transfer chromophores is reported comprising a square-planar nickel(II) with one catecholate donor ligand and one α-diimine acceptor ligand in a coplanar arrangement. An intense ligand-to-ligand charge-transfer (LL′CT) absorption band that can be tuned from 650 nm (1.9 eV) to 1370 nm (0.9 eV) and a rich ground-state redox chemistry distinguish these complexes as attractive candidates for charge-transfer photochemistry and solar-energy conversion applications.

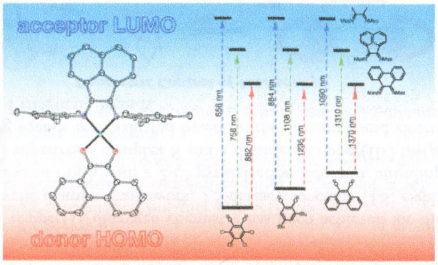

Additions and Corrections

8838 dx.doi.org/10.1021/ic501773f

Correction to Octakis(*tert*-butoxo)dicerium(IV) $[Ce_2(O^tBu)_8]$: Synthesis, Characterization, Decomposition, and Reactivity

Johannes Schläfer, Wieland Tyrra, and Sanjay Mathur*

S Supporting Information available via online article